



Impact of the Loess Plateau on the atmospheric boundary layer structure and air quality in the North China Plain: A case study



Xiao-Ming Hu^a, ZhiQiang Ma^{b,*}, Weili Lin^c, Hongliang Zhang^d, Jianlin Hu^d, Ying Wang^c, Xiaobin Xu^c, Jose D. Fuentes^e, Ming Xue^a

^a Center for Analysis and Prediction of Storms, and School of Meteorology, University of Oklahoma, Norman, OK 73072, USA

^b Institute of Urban Meteorology, China Meteorological Administration, Beijing 100089, China

^c Key Laboratory for Atmospheric Chemistry, Center for Atmospheric Watch and Services, Chinese Academy of Meteorological Sciences, Beijing, 100081, China

^d Department of Civil & Environmental Engineering, University of California, Davis, CA 95616, USA

^e Department of Meteorology, Pennsylvania State University, University Park, PA 16802, USA

HIGHLIGHTS

- Low mixed layer exacerbates air pollution over the North China Plain (NCP)
- Warm advection from the Loess Plateau leads to the lid formation over the NCP
- The Mountain-Plains Solenoid (MPS) circulation also suppresses the mixed layer.
- Different heating between Plateau and Plain affects boundary layer structure.

ARTICLE INFO

Article history:

Received 3 July 2014

Received in revised form 15 August 2014

Accepted 18 August 2014

Available online 3 September 2014

Editor: Xuexi Tie

Keywords:

North China Plain

Ozonesonde

WRF/CMAQ

Atmospheric boundary layer

Air pollution

Westerly warm advection

ABSTRACT

The North China Plain (NCP), to the east of the Loess Plateau, experiences severe regional air pollution. During the daytime in the summer, the Loess Plateau acts as an elevated heat source. The impacts of such a thermal effect on meteorological phenomena (e.g., waves, precipitation) in this region have been discussed. However, its impacts on the atmospheric boundary layer structure and air quality have not been reported.

It is hypothesized that the thermal effect of the Plateau likely modulates the boundary layer structure and ambient concentrations of pollutants over the NCP under certain meteorological conditions. Thus, this study investigates such effect and its impacts using measurements and three-dimensional model simulations. It is found that in the presence of daytime westerly wind in the lower troposphere (~1 km above the NCP), warmer air above the Loess Plateau was transported over the NCP and imposed a thermal inversion above the mixed boundary layer, which acted as a lid and suppressed the mixed layer growth. As a result, pollutants accumulated in the shallow mixed layer and ozone was efficiently produced. The downward branch of the thermally-induced Mountain-Plains Solenoid circulation over the NCP contributed to enhancing the capping inversion and exacerbating air pollution. Previous studies have reported that low mixed layer, a factor for elevated pollution in the NCP, may be caused by aerosol scattering and absorption of solar radiation, frontal inversion, and large scale subsidence. The present study revealed a different mechanism (i.e., westerly warm advection) for the suppression of the mixed layer in summer NCP, which caused severe O₃ pollution. This study has important implications for understanding the essential meteorological factors for pollution episodes in this region and forecasting these severe events.

© 2014 Elsevier B.V. All rights reserved.

1. Introduction

Regional air pollution in terms of both ozone (O₃) and particulate matter (PM) in the North China Plain (NCP) has become one of the top environmental issues in China (He et al., 2001; Hao et al., 2005;

Sun et al., 2006; Ding et al., 2008; Lin et al., 2008; Meng et al., 2009; Xu et al., 2011b; Zhao et al., 2011; Ma et al., 2012a,b; Huang et al., 2013; Lang et al., 2013; Chen et al., 2013; Hu et al., 2014). In addition to direct emissions (see NO_x emission in Fig. 1a), meteorological conditions also play an important role in modulating ambient concentrations of pollutants in this region (Su et al., 2004; Chen et al., 2008; Zhang et al., 2009; Wang et al., 2009; Wang et al., 2010b; Gao et al., 2011; Wei et al., 2011; Yang et al., 2011; Zhang et al., 2012; Ji et al., 2012, 2014). A few

* Corresponding author. Tel.: +86 10 68400757.

E-mail addresses: xhu@ou.edu (X.-M. Hu), zqma@ium.cn (Z. Ma).

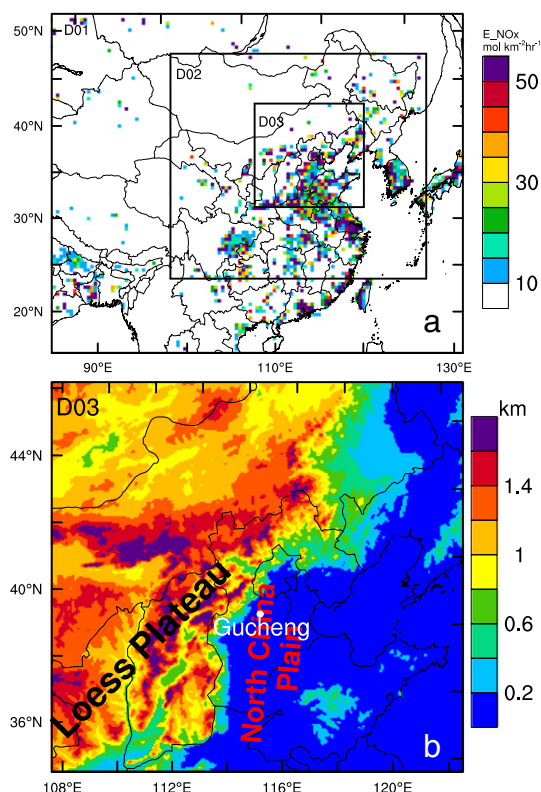


Fig. 1. (a) Domain configuration for the WRF simulation overlaid with NO_x emission rates composed in Zhang et al. (2012) and (b) detailed terrain distribution around the North China Plain in domain 3. The location of the Gucheng research site is marked in panel b.

recent studies investigated the relationship between synoptic weather patterns and air quality in the NCP. It was concluded that variation of the synoptic patterns modulated the abundance of ambient pollutants and likely provided the primary driving force for the day-to-day variations in regional pollutant concentrations (Chen et al., 2008; Wang et al., 2009; Zhang et al., 2012; Wei et al., 2011). Southwesterly surface wind was found more likely to lead to severe air pollution in the NCP (e.g., Chen et al., 2008; Wang et al., 2010a; Xu et al., 2011a; Wang et al., 2013b; Zhang et al., 2012). However, only few studies investigated the atmospheric boundary layer structure and its impact on air quality in this region (Quan et al., 2014). Previous studies did not ascribe the root causes of the day-to-day variation of pollutants in the NCP to the different boundary layer structures. The thermal and dynamic characteristics of the atmospheric boundary layer and their relationship with air pollution in the NCP remain to be further studied (Liu et al., 2013; Zhao et al., 2013). One objective of the present study is to reveal the crucial role of the atmospheric boundary layer structure and air flow above the surface (in addition to the surface wind) in causing severe air pollution in this region.

The Loess Plateau, with altitudes of 1000–2000 m above sea level (asl), is located to the west of the NCP (with altitudes of less than 50 m asl) (Fig. 1b). During the daytime in the summer, the Loess Plateau acts as an elevated heat source in the vicinity of the low-lying NCP (He and Zhang, 2010; Sun and Zhang, 2012). Due to intense solar radiation,

the near-surface air temperature over the Plateau is normally higher than air temperature at the same height over the adjacent Plains (Gao et al., 1981). This thermal effect of the Plateau likely modulates the atmospheric boundary layer structures over the NCP under certain meteorological conditions. While much effort has been made in understanding impacts of different heating/cooling between mountains and adjacent plains on meteorological phenomena such as waves and precipitation (e.g., Tripoli and Cotton, 1989; Wolyn and Mckee, 1994; Zhang and Koch, 2000; Koch et al., 2001; Zaitchik et al., 2007; Carbone and Tuttle, 2008; He and Zhang, 2010; Sun and Zhang, 2012; Bao and Zhang, 2013), its impacts on the atmospheric boundary layer structure and air quality remain poorly understood (Lanucci and Warner, 1991, 1997; Luke et al., 1992; Ryan et al., 1992; Warner and Sheu, 2000; Pagnotti, 1987; Seaman and Michelson, 2000).

Resulting from heating over the Plateau and sloping terrains during the afternoon in summer and autumn months, upslope wind develops along the sloping terrains. Simultaneously, a downward return flow develops over the adjacent Plains. Such thermally driven phenomenon is termed the Mountain-Plains Solenoid (MPS) circulation (Tripoli and Cotton, 1989; May and Wilczak, 1993; Sun and Zhang, 2012). A few studies (e.g., Liu et al., 2009; He and Zhang, 2010; Sun and Zhang, 2012; Bao and Zhang, 2013; Zhang et al., 2014) reported that precipitation occurs on the slopes of the Plateaus usually during midday or early afternoon associated with the upward branch of the MPS circulation and propagates to the adjacent Plains during the nighttime. This study will extend previous investigations to illustrate the impact of MPS on the atmospheric boundary layer structure and air quality.

During summer 2013, a research field campaign was conducted at Gucheng, a rural site in the north part of the NCP (Fig. 1b). Vertical profiles of chemical and meteorological variables were measured in addition to surface measurements. These data together with three-dimensional air quality simulation results are analyzed in this study to investigate the impacts of the thermal effects of the Loess Plateau on the atmospheric boundary layer structure and the O₃ concentrations in the NCP.

2. Methods

2.1. In-situ measurements at Gucheng

2.1.1. Site description

The Gucheng site (39°08'N, 115°40'E, 15.2 m asl) in Hebei Province is an Integrated Ecological-Meteorological Observation and Experiment Station of the Chinese Academy of Meteorological Sciences. The site is located in the northern part of the NCP, ~120 km southwest of the Beijing–Tianjin metropolitan area, 35 km north of the Baoding city (Fig. 1b). The Gucheng site is surrounded by farms, villages/towns, and transportation network in the NCP. The main crop around this site is corn in the summer and fall (Lin et al., 2009). Starting from the summer of 2006, several institutions have measured atmospheric chemical species near the surface at Gucheng, in order to monitor regional background concentrations of air pollutants in the NCP (Lin et al., 2009; Wang et al., 2013a).

2.1.2. Field experiment in the summer of 2013

In the summer of 2013, instruments from Thermo Environmental Instruments, Inc. were used to measure ground-level chemical species at Gucheng, including O₃ (model TE 49C), CO (TE 48C), NH₃ (DLT-100),

Table 1

Sigma levels and mid-layer heights (m AGL) of the lowest 20 WRF model layers.

Sigma levels	1.0	0.997	0.994	0.991	0.988	0.985	0.975	0.97	0.96	0.95
Mid-layer heights	12	37	61	86	111	144	186	227	290	374
Sigma levels	0.94	0.93	0.92	0.91	0.895	0.88	0.865	0.85	0.825	0.8
Mid-layer heights	459	545	631	717	826	958	1092	1226	1409	1640

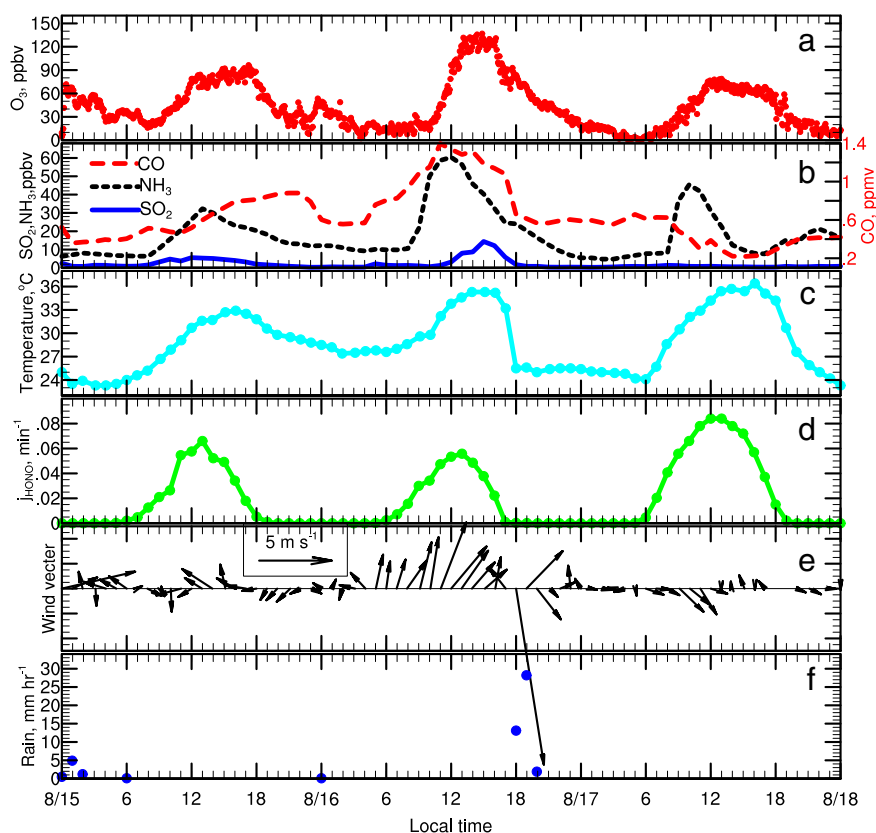


Fig. 2. Surface (a) O_3 , (b) SO_2 , NH_3 , CO , (c) temperature, (d) photolysis rate coefficients of HONO (j_{HONO}), (e) wind vector, and (f) hourly rain rate measured at Gucheng on August 15–17, 2013.

and SO_2 (TE 43CTL). Surface meteorological data were also recorded. The photolysis rate coefficient of HONO (j_{HONO}), which is proportional to the shortwave radiation, was measured using a 2-pi-actinic-flux spectrograph (Meteorologie Consult GmbH, Germany). In addition to the surface measurements, vertical profiles of O_3 , temperature, humidity, and winds were measured up to ~ 1 km above the surface at Gucheng using balloon-borne meteorological and O_3 sondes during several intensive observation periods (IOPs) in August and September, 2013. The ozonesondes were of the Brewer–Mast design consisting of a single cell containing a buffered potassium iodide solution which generates a current when ozone is bubbled through the cell with a constant volume pump, which are known to have accuracy of 5–10% in the troposphere (Brewer and Milford, 1960; Stubi et al., 2008). A similar set-up was used to measure O_3 concentrations and meteorological variables

in the lower troposphere in a few other locations including the Beijing and Washington, D.C. metropolitan area (Ma et al., 2011b, 2013; Hu et al., 2012, 2013a). Ozone and meteorological data (i.e., wind speed and direction, temperature, pressure, and humidity) were transmitted to a ground receiver every second. One of the IOPs coincides with the day with the highest O_3 concentration in August and September 2013 recorded at the research site (i.e., 137 ppbv on August 16). Thus this episode is chosen for a detailed analysis.

2.2. Ozone measurements at cities in the NCP

Independently of the 2013 summer field experiment at Gucheng, O_3 concentrations at more than 100 cities in China are routinely measured and posted online by the Chinese Ministry of Environmental Protection (MEP). Ozone values at seven cities in the NCP, i.e., Handan (HD), Hengshui (HS), Shijiazhuang (SJZ), Baoding (BD), Jinan (JN), Cangzhou (CZ), Tianjin (TJ), are analyzed to examine O_3 spatial distribution and the likely causes.

2.3. Three-dimensional simulation

To investigate the atmospheric boundary layer structure and its impact on air quality for the selected episode (i.e., August 16–17, 2013), three-dimensional air quality simulations with the Weather Research and Forecast (WRF) (version 3.5.1)/Community Multiscale Air Quality (CMAQ) (version 4.7.1) models were conducted. For the WRF simulations, three one-way nested domains (Fig. 1a) were employed with horizontal grid resolutions of 40.5, 13.5, and 4.5 km, respectively. Each domain had 48 vertical layers extending from the surface to 100 hPa. The sigma levels and mid-layer heights of the lowest 20 model layers are shown in Table 1. All model domains used the Dudhia shortwave radiation algorithm (Dudhia, 1989), the rapid radiative transfer model

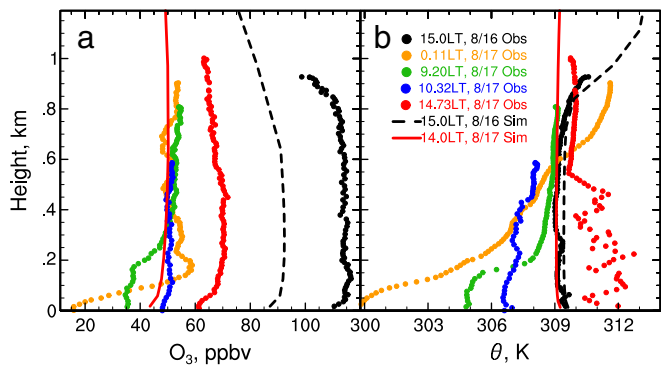


Fig. 3. Vertical profiles of (a) O_3 and (b) potential temperature (θ) at the Gucheng research site measured by tethered balloons (dots) and simulated by the WRF/CMAQ models (lines). Note the tethered balloon was only launched to ~ 1 km above the ground.

(Mlawer et al., 1997) for longwave radiation, the WRF Single-Moment 6-class (WSM6) microphysics scheme (Hong et al., 2004), and the Noah land-surface scheme (Chen and Dudhia, 2001). Similar model configurations were used in previous studies of the atmospheric boundary layer (e.g., Hu et al., 2013b). Planetary boundary layer (PBL) parameterization scheme is a critical model component to correctly simulate the atmospheric boundary layer (Hu et al., 2010a, 2013c). The Younsei

University (YSU) PBL scheme (Hong et al., 2006) was demonstrated to perform well for both daytime and nighttime (Hu et al., 2013c), and thus it was selected for the simulations presented in this study. The $1^\circ \times 1^\circ$ National Centers for Environmental Prediction (NCEP) Final (FNL) Global Forecast System (GFS) operational analyses were used for the initial and boundary conditions of all meteorological variables. Different meteorological spin-up (or initial meteorological conditions) was reported to affect ozone simulation (Zhang et al., 2007). Thus the effect of different spin-up times was tested, three 60-h simulations were initialized at 1200 UTC (UTC = Local time – 8 h), 1800 UTC August 15, and 0000 UTC August 16, respectively. The simulation initiated at 0000 UTC August 16 showed the best overall performance based on the comparison with the observations in terms of front positions, and its results are thus analyzed in this manuscript to reveal the meteorological factors contributing to the O_3 episode. This approach was applied in an earlier study (Hu et al., 2013d) to investigate the meteorological cause for the secondary O_3 peak associated with a cold front passage.

For the offline CMAQ simulation, which is driven by the WRF simulated meteorological fields, only the outer two nested domains were employed and other configurations (e.g., vertical layers, chemical mechanism, etc.) followed an earlier study of Zhang et al. (2012). Anthropogenic emissions were generated from the Emission Database for Global Atmospheric Research (EDGAR) inventory v4.2 (available at <http://edgar.jrc.ec.europa.eu/overview.php?v=42>) and biogenic emissions were predicted using Model of Emissions of Gases and Aerosols from Nature (MEGAN) v2.04 (Guenther et al., 2006). Details about the emission generation can be found in Wang et al. (2014).

3. Results

The highest O_3 mixing ratios at Gucheng during August and September, 2013 (~137 ppbv) occurred between 1300 and 1600 Local Time (LT), August 16, which were substantially higher than the maximum O_3 mixing ratios on August 15 and 17 (Figs. 2a, 3a). Short wave radiation and temperature are the most critical meteorological factors dictating the O_3 formation reactions with stronger radiation and higher temperature normally leading to more efficient O_3 production. However, surface radiation/temperature on August 16 was not the strongest/highest in August and September (Fig. 2c, d). In fact, radiation on this day was weaker than the preceding and subsequent days, indicated by variation of j_{HONO} (Fig. 2d). Thus, other factors (rather than radiation and temperature) must play roles in contributing to O_3 accumulation in the NCP on August 16. Different atmospheric boundary layer heights have been reported to modulate day-to-day variation of ground-level ozone concentration in different regions (e.g., Hu et al., 2010b; Haman et al., 2014). The boundary layer structure needs to be taken into account when interpreting surface concentrations of pollutants (Culf et al., 1997), it is thus examined for the selected O_3 episode in the following paragraphs.

Prominently higher O_3 concentration and its well-mixed vertical distribution in the daytime convective boundary layer in polluted region have been used to diagnose the atmospheric boundary layer structure (e.g., Hu et al., 2012, 2013a). Ozone mixing ratios in the lower part of the boundary layer (<~800 m above the surface) at 1500 LT on August 16 were nearly uniformly as high as ~115 ppbv (except positive gradient near the surface), indicating accumulation of O_3 in the convective boundary layer (Fig. 3a). Above it, the O_3 mixing ratio decreased, indicating a transition from the polluted convective boundary layer to the cleaner free troposphere. Such boundary layer structure diagnosis from the O_3 profile is consistent with what is implied by the observed profile of potential temperature (θ). A potential temperature inversion at ~800–900 m above the surface at 1500 LT indicated the top of the convective boundary layer (Fig. 3b). The mixed layer height diagnosed from the observed potential temperature profile using the 1.5-theta-increase method (Hu et al., 2010a, 2013a) is 925 m at 1500 LT, August 16. Note that the 1.5-theta-increase method defines mixed

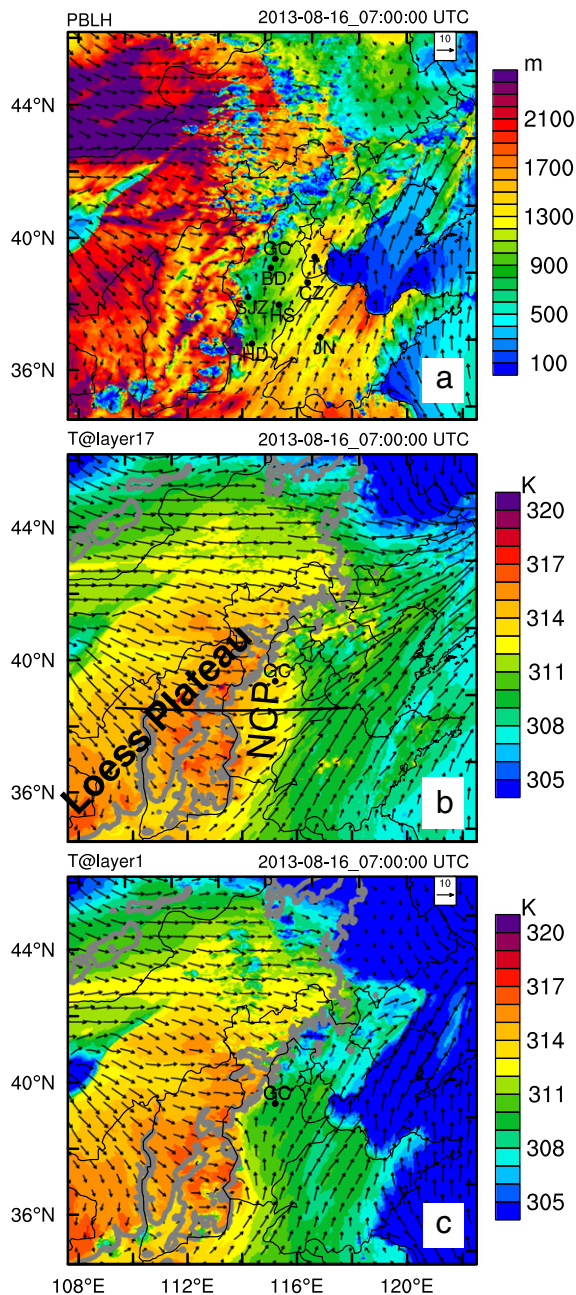


Fig. 4. Spatial distribution of (a) planetary boundary layer (PBL) height, and potential temperature (b) at the 17th model layer (~1200 m above the NCP) and (c) at the 1st model layer at 0700 UTC (1500 LT), August 16, 2013 simulated by WRF. Note that PBL and the mixed layer are interchangeable during the daytime. Simulated surface wind vectors are overlaid on panels a and c and wind vectors at the 17th model layer are overlaid on the panel b. Seven cities are marked in panel a, i.e., Handan (HD), Hengshui (HS), Shijiazhuang (SJZ), Baoding (BD), Jinan (JN), Cangzhou (CZ), Tianjin (TJ), where O_3 concentrations are routinely measured by the Chinese Ministry of Environmental Protection. The 900 m terrain elevation is plotted on panels b and c in thick gray curves denoting the approximate location of the steepest terrain slope. The horizontal straight black line in panel b represents the location of cross sections shown in Fig. 9. The location of Gucheng (GC) is marked in each panel.

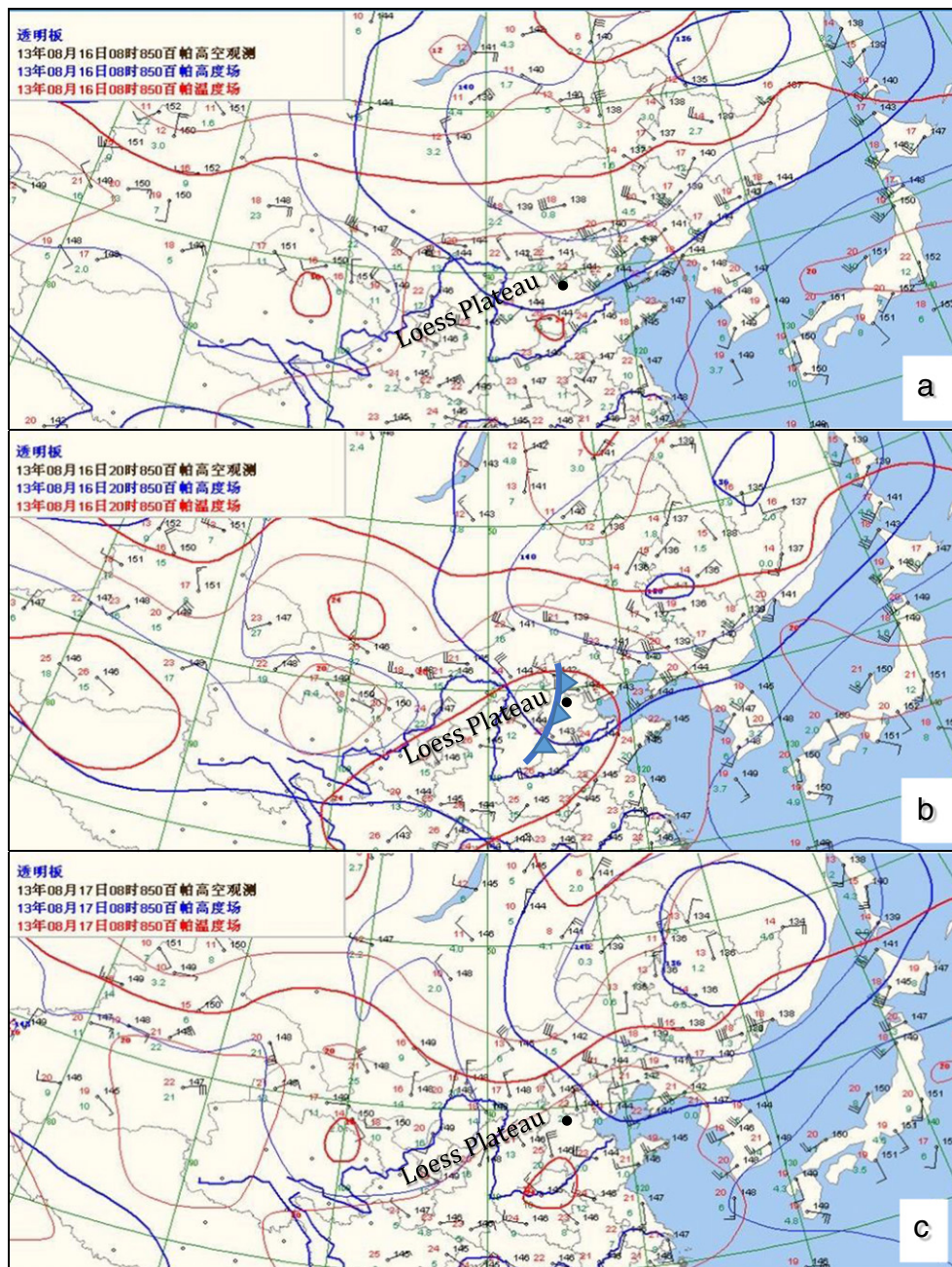


Fig. 5. Weather map at 850 hPa at (a) 0800 LT, August 16, (b) 2000 LT, August 16, and (c) 0800 LT, August 17, 2013 based on the MICAPS (Meteorological Information Comprehensive Analysis and Process) observation data archived by China Meteorological Administration. The blue lines are isopleths of geopotential height and the red lines are isotherms. The location of Gucheng is marked by black dots.

layer top as the level at which the potential temperature first exceeds the minimum potential temperature within the boundary layer by 1.5 K (Nielsen-Gammon et al., 2008). The WRF simulation reproduced the observed boundary layer structure quite well, as indicated by the simulated temperature profile nicely resembling observation (Fig. 3b). The simulated mixed layer height at 1500 LT on August 16 is 912 m. The mixed layer top on the afternoon of August 16 is much lower than that on the afternoon of August 17. The simulated mixed layer height at 1400 LT on August 17 is 1821 m. Since the tethered balloon was only launched to ~1 km above the ground, mixed layer top cannot be diagnosed from the observed profile on the afternoon of August 17 (Fig. 3b). The reason for the large variation of θ in the lower mixed layer (<600 m above the ground) at 14.73 LT, August 17 needs further investigation, but is beyond the scope of this study.

The relatively shallow mixed layer on the afternoon of August 16 played an important role for the accumulation of boundary layer pollutants. A few primary pollutants with relatively long lifetimes (e.g., CO, SO₂, and NH₃) showed elevated surface mixing ratios on August 16 comparing to the preceding and subsequent days (Fig. 2b). The ambient concentrations of these primary pollutants are largely modulated by dispersion after they are emitted into the atmosphere. The much lower mixed layer on August 16 limited the total dispersion volume and resulted in higher concentrations of these species. Similarly, enhanced concentrations of NO_x and volatile organic compounds (which are the precursors of tropospheric O₃) occurred on the afternoon of August 16 due to the suppressed dispersion, increased the O₃ production efficiency and caused high O₃ concentrations. The CMAQ simulation generally captures the

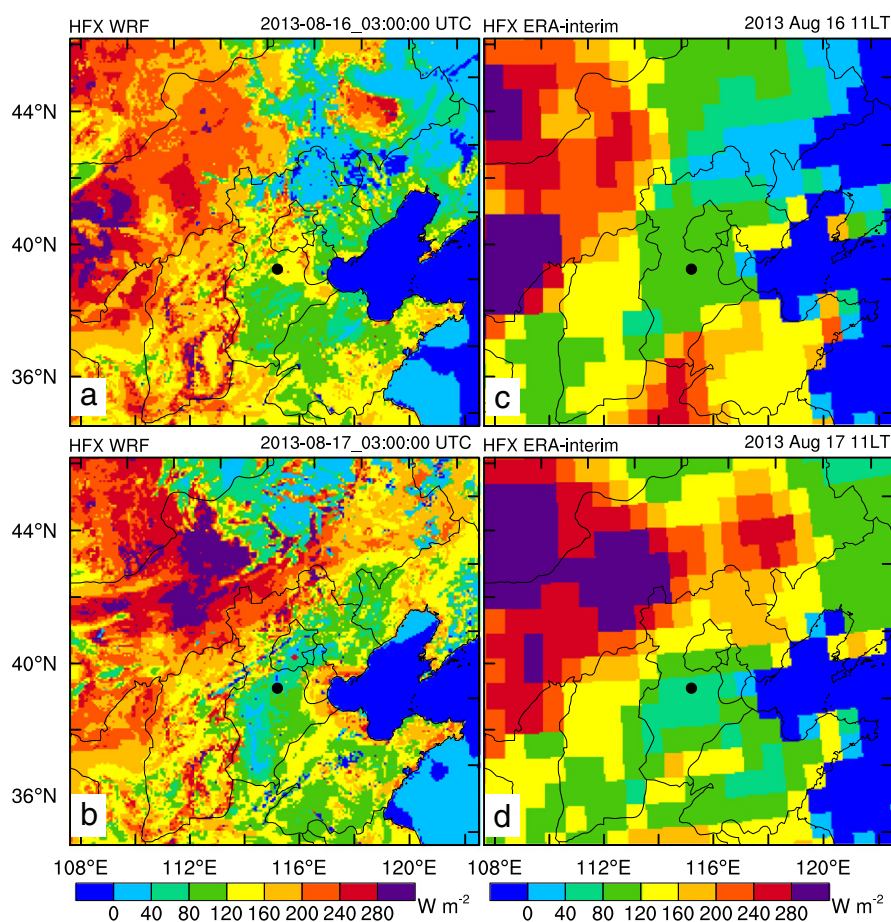


Fig. 6. Upward sensible heat flux (HFX) (a, b) simulated by WRF and (c, d) derived from the ERA-Interim data (archived at http://data-portal.ecmwf.int/data/d/interim_full_daily/) at 0300 UTC (1100 LT) on (top) August 16 and (bottom) August 17, 2013. The location of Gucheng is marked by black dots.

characteristics of vertical profiles of O_3 (Fig. 3a). The slightly lower mixed layer height at 1500LT August 16 indicated by simulated O_3 profile, compared to that indicated by the observed O_3 profile, is partially due to relatively coarser vertical resolution employed in the CMAQ simulation than in the WRF simulation (Zhang et al., 2012). A systematic underestimation of O_3 (~20 ppbv) is noticed due to the uncertainties in the China emissions (Zhang et al., 2012).

The WRF simulation (Fig. 4a) indicated that the low mixed layer height on the afternoon of August 16 was not limited to the measurement site. Instead, it covered a large portion of the NCP, spanning ~200 km east of the Loess Plateau. Southerly wind in this region dominated near the surface (Figs. 4a, 2e), while westerly and northwesterly surface wind dominated over the Loess Plateau (Fig. 4a). The MICAPS (Meteorological Information Comprehensive Analysis and Process) observation data archived by China Meteorological Administration also confirm such a surface weather pattern (not shown) and a trough at 850 hPa above the west part of NCP (Fig. 5). Both the veering of the wind field (Fig. 4a) and the trough (Fig. 5b) indicate a front along the east edge of the Loess Plateau. The preceding part of fronts has been reported to be often associated with enhanced air pollution in northern China in a synoptic climatology study of Chen et al. (2008) and an air quality modeling study of Wang et al. (2010a). These studies, however, did not reveal the cause in the boundary layer structure for exacerbation of air pollution under such a synoptic pattern.

Soil moisture was reported to affect the atmospheric boundary layer structure through modulating partitioning of incoming solar radiation energy between sensible and latent heat flux (Ma et al., 2011a). Generally low/high soil moisture content partitions more/less surface available energy into sensible heat flux, as a result leading to high/low daytime

boundary layer (e.g., Hu et al., 2010a; Ma et al., 2011a; Westra et al., 2012; Sandeep et al., 2014). To examine such a possible cause for the low mixed layer height on August 16, surface sensible heat flux (HFX) simulated by WRF and derived from the European Centre for Medium-range Weather Forecasts (ECMWF) ERA-interim data is investigated. HFX at 1100 LT (when the mixed layer rapidly grows) from WRF and ERA-interim show similar spatial distributions on August 16 and 17 with lower HFX over the NCP and higher HFX to the west and northwest of NCP, even though discrepancies can be noticed (Fig. 6). Both WRF and ERA-interim have relatively higher HFX around Gucheng on August 16 (Fig. 6a, c) than August 17, 2013 (Fig. 6b, d). Thus surface HFX cannot explain the relatively lower mixed layer heights around Gucheng on August 16 comparing to August 17.

During summer daytime, plateaus often act as elevated heat sources due to absorption of intense solar radiation and their near-surface air temperature is higher than the air temperature at the same altitude in the neighborhood in the absence of advection (Gao et al., 1981; Ye, 1981). WRF simulated temperature fields clearly illustrate that the Tibetan Plateau (referred to as the “first step” terrain in China, see terrain heights in Fig. 7a) is the heat source at 550 hPa (Fig. 7c) and the Loess Plateau (referred to as the “second step” terrain in China) is the heat source at 850 hPa (Fig. 7b). Note that the temperature contours in Fig. 7b and c do not exactly match the terrain contours in Fig. 7a due to horizontal advection of temperature.

In the presence of westerly wind, the heat source of the Loess Plateau affected the boundary layer structure in its eastern neighborhood, i.e., in the NCP. The simulated fields of potential temperature and wind vector at the 17th model layer (~1200 m above the ground over the NCP) show warm advection over the areas with relatively low mixed

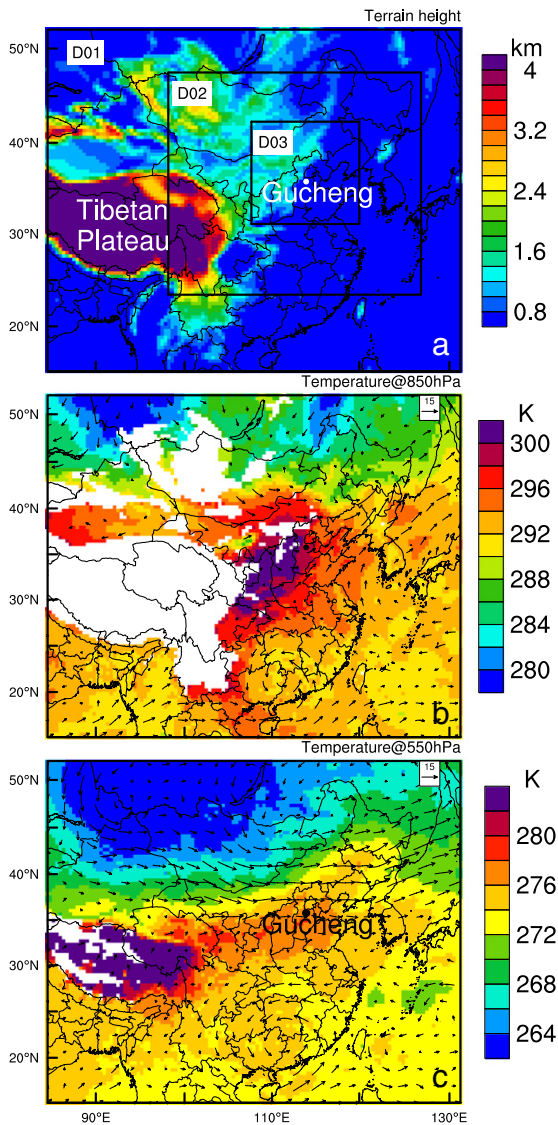


Fig. 7. (a) Terrain height, (b) temperature and wind field at 850 hPa, and (c) temperature and wind field at 550 hPa at 0700 UTC (1500 LT), August 16, 2013 interpolated from WRF outputs. Blank area in panels b and c means the terrain heights at those area are higher than the heights of 850 hPa and 550 hPa, respectively.

layers (Fig. 4b). Westerly wind advects the warm air from the Plateau eastward to the NCP and creates a strong temperature inversion above the boundary layer (Fig. 3b) while relatively colder air persists in the boundary layer above NCP (Fig. 4c). The temperature inversion acts as a lid, suppressing the development of the mixed layer (the mixed layer height on the afternoon of August 16 was only ~900 m above the ground, Fig. 3) and limiting the dispersion of boundary layer pollutants. As a result, pollutants accumulated in the atmospheric boundary layer and O_3 was efficiently produced (Fig. 2a, b). The time sequence of the westerly warm advection is also examined. It started and was relatively weak in the early morning. The warm advection became most prominent in the afternoon (Fig. 4b) and it disappeared when the cold front passed by during the early evening of August 16 (figure not shown). Thus the mixed layer was suppressed for the whole day and it never grew higher than 1 km. On August 17, the trough at 850 hPa moved eastward to the East Sea and northerly wind dominated over the NCP (Fig. 5). The lid formation mechanism (i.e., westerly warm advection) broke down and the mixed layer developed to a higher altitude (The simulated mixed layer height on the

afternoon of August 17 is as high as 1821 m). Thus the boundary layer pollutants dispersed and lower O_3 persisted on August 17 than August 16, 2013 (Figs. 2, 3).

The spatial distribution of O_3 is investigated using the data at the seven cities in the NCP collected by the MEP (Fig. 8). Four cities in the west of the NCP (i.e., HD, HS, SJZ, BD) showed higher O_3 mixing ratios on August 16 than the preceding and subsequent days (Fig. 8a) while three cities in the east (i.e., JN, CZ, TJ) experienced lower values on this day (Fig. 8b). Southerly or southwesterly wind persisted over all the seven cities on the afternoon of August 16, 2013 (Fig. 4a). Thus the southerly/southwesterly advection is unlikely the main factor contributing to the higher O_3 on August 16 in the west of the NCP. The four cities in the west of the NCP experiencing high O_3 on August 16 were affected by the westerly warm advection (Fig. 4b) and had low mixed layers, while the three cities to the east experiencing relatively lower O_3 had relatively higher mixed layers (Fig. 4a). Such correlation between O_3 mixing ratios and mixed layer height further confirmed that the atmospheric boundary layer structure played an important role in leading to the elevated O_3 concentrations in the west of the NCP (an area spanning ~200 km from west to east) on August 16, 2013.

To the best of our knowledge, none of the existing studies investigated the summertime atmospheric boundary layer structure and its impact on ozone air quality in the NCP. Quan et al. (2014) investigated the characteristics of heavy aerosol pollution in wintertime Beijing, which is located at the northern edge of the NCP. It was found that solar radiation reduction through aerosol scattering and absorption suppressed the development of the mixed layer (Quan et al., 2013, 2014) and the low mixed layer height played an important role in causing the heavy aerosol pollution in winter Beijing. Zhang et al. (2009) analyzed aerosol profiles measured by aircrafts in spring Beijing and found that frontal inversions led to high aerosol concentrations in low boundary layers. The data reported in Liu et al. (2013) appears to suggest that low boundary layer partially caused an air pollution episode (in terms of both O_3 and aerosols) around Beijing in September 2011 and the low boundary layer was speculated to be due to subsidence associated with large scale high pressure. Our study revealed a different mechanism (i.e., westerly warm advection) for the suppression of the mixed layer in summer NCP, which caused severe O_3 pollution.

Westerly warm advection is also demonstrated in the vertical west-to-east cross section (Fig. 9a, b). Superimposed upon the westerly advection, the MPS circulation is evident (Fig. 9c, d). Due to the solar heating in the afternoon, an upward motion occurs on the eastern slope of the Plateau. Simultaneously a downward motion occurs on

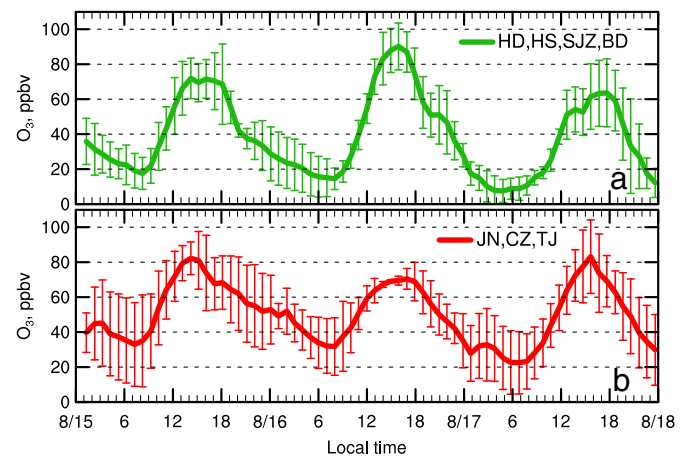


Fig. 8. Mean O_3 mixing ratios and standard deviations (a) at the cities with low mixed layer height (i.e., HD, HS, SJZ, BD) and (b) at the cities with relatively higher mixed layer height (i.e., JN, CZ, TJ) in the NCP on August 16, 2013. The locations of the seven cities are marked in Fig. 4a.

the NCP, which is prominent in an area about ~200 km wide (Fig. 9c, d). The downward branch of the MPS circulation contributes to enhance the capping inversion above the boundary layer and effectively caps the relatively cool and low mixed layer over the NCP (Fig. 9a, b). As a result, pollutants accumulated in the shallow mixed layer (Figs. 2a, b, 3a). The impact of MPS circulation on diurnal variation of precipitation was actively investigated recently (e.g., Liu et al., 2009; He and Zhang, 2010; Sun and Zhang, 2012; Bao and Zhang, 2013; Zhang et al., 2014). To our knowledge, this study is the first attempt to attribute air pollution episodes in the NCP partially to the MPS circulation. Under favorable conditions, the upward branch of the MPS circulation triggers precipitation on the eastern slopes of the Loess Plateau during midday or afternoon, which subsequently propagates eastward or southeastward to the NCP (He and Zhang, 2010; Sun and Zhang, 2012; Bao and Zhang, 2013). Though not shown here, we examined the high-resolution precipitation products obtained from the Climate Prediction Center's morphing technique (CMORPH). Patches of precipitation indeed occurred over the slope of the Plateau northwest to the Gucheng research site in the afternoon of August 16, 2013 and propagated to the research site during the early evening transition as also recorded at the surface site (Fig. 2f). These precipitation characteristics further confirmed the occurrence of the MPS circulation, which contributed to exacerbating the air pollution in the NCP on August 16, 2013.

4. Conclusions and discussions

This study investigates the impacts of the thermal effect of the Loess Plateau on the atmospheric boundary layer structure and air quality over the NCP using in-situ measurements and three-dimensional WRF/CMAQ simulations. During summer daytime, the Loess Plateau acts as an elevated heat source. In the presence of westerly wind in the lower troposphere (~1 km above the NCP), warmer air above the Loess Plateau was advected eastward and imposed a thermal inversion above the mixed boundary layer in the west part of the NCP (an area spanning ~200 km from west to east), which acted as a lid and suppressed the mixed layer growth. As a result, pollutants accumulated in a relatively lower mixed layer and O₃ was efficiently produced. Superimposed upon the westerly warm advection, the downward branch of the MPS circulation over the NCP contributed to strengthen the capping inversion above the mixed layer. The spatial distribution of O₃ and its relationship with that of the mixed layer height further confirmed the important role of mixed layer height in O₃ accumulation in the NCP.

The southwest transport pathway near the surface was identified in a few studies (e.g., Chen et al., 2008; Wang et al., 2010a; Wang et al., 2013b; Zhang et al., 2012) to be usually associated with severe air pollution in the NCP. Measurements of vertical profiles of meteorological variables and chemical species were not available for these studies at

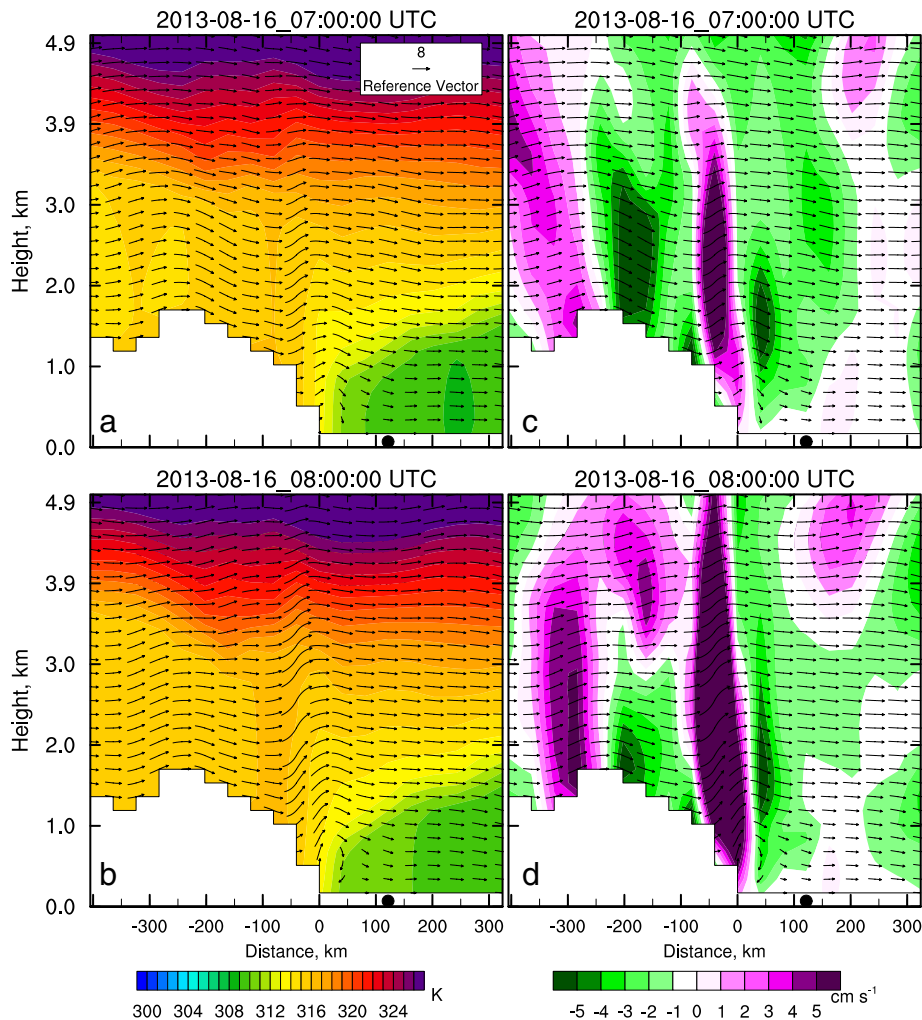


Fig. 9. West-to-east vertical cross sections of (a, b) potential temperature and (c, d) vertical velocity through the North China Plain at (top) 0700 UTC (1500 LT) and (bottom) 0800 UTC (1600 LT), August 16, 2013. The location of the cross section is marked in Fig. 4b. Wind vectors are overlaid on each plot. Note that vertical velocity is multiplied by 100 when plotting wind vectors. The longitudinal position of the Gucheng research site is marked by a black dot on the x-axis.

that time. Thus, they did not attribute the cause of the regional air pollution to the boundary layer structure. This study indicates that the surface southwesterly wind in the NCP could be associated with a trough above the west part of the NCP. Thus westerly or northwesterly wind could dominate over the Loess Plateau and daytime westerly warm advection in the low troposphere likely leads to formation of a thermal inversion over the low mixed layer above the NCP, which inhibits mixed layer growth and causes regional air pollution eventually. Thus, air flow above the surface and the boundary layer structure need to be paid careful attention to in addition to surface wind fields when investigating the air quality issues in the NCP.

Acknowledgment

This work was supported by the National Natural Science Foundation of China under grant no. 41105092, the China Special Fund for Meteorological Research in the Public Interest (No. GYHY201206015), and Beijing Natural Science Foundation (8121002). Proofreading by David C. Doughty is greatly appreciated. Xu Lu provided the weather map.

References

- Bao XH, Zhang FQ. Impacts of the mountain-plains solenoid and cold pool dynamics on the diurnal variation of warm-season precipitation over northern China. *Atmos Chem Phys* 2013;13:6965–82.
- Brewer AW, Milford JR. The Oxford-Kew ozone Sonde. *Proc R Soc Lond A* 1960;256:470–95.
- Carbone RE, Tuttle JD. Rainfall occurrence in the US warm season: the diurnal cycle. *J Clim* 2008;21:4132–46.
- Chen F, Dudhia J. Coupling an advanced land surface-hydrology model with the Penn State-NCAR MM5 modeling system. Part I: model implementation and sensitivity. *Mon Weather Rev* 2001;129:569–85.
- Chen ZH, Cheng SY, Li JB, Guo XR, Wang WH, Chen DS. Relationship between atmospheric pollution processes and synoptic pressure patterns in northern China. *Atmos Environ* 2008;42:6078–87.
- Chen PF, Quan JN, Zhang Q, Tie XX, Gao Y, Li X, et al. Measurements of vertical and horizontal distributions of ozone over Beijing from 2007 to 2010. *Atmos Environ* 2013;74:37–44.
- Culf AD, Fisch G, Malhi Y, Nobre CA. The influence of the atmospheric boundary layer on carbon dioxide concentrations over a tropical forest. *Agr Forest Meteorol* 1997;85:149–58.
- Ding AJ, Wang T, Thouret V, Cammas JP, Nedelec P. Tropospheric ozone climatology over Beijing: analysis of aircraft data from the MOZAIC program. *Atmos Chem Phys* 2008;8:1–13.
- Dudhia J. Numerical study of convection observed during the winter monsoon experiment using a mesoscale two-dimensional model. *J Atmos Sci* 1989;46:3077–107.
- Gao YX, Tang MC, Luo SW, Shen ZB, Li C. Some aspects of recent research on the Qinghai-Xizang plateau meteorology. *Bull Am Meteorol Soc* 1981;62:31–5.
- Gao Y, Liu X, Zhao C, Zhang M. Emission controls versus meteorological conditions in determining aerosol concentrations in Beijing during the 2008 Olympic Games. *Atmos Chem Phys* 2011;11:12437–51.
- Guenther A, Karl T, Harley P, Wiedinmyer C, Palmer PI, Geron C. Estimates of global terrestrial isoprene emissions using MEGAN (Model of Emissions of Gases and Aerosols from Nature). *Atmos Chem Phys* 2006;6:3181–210.
- Haman CL, Couzo E, Flynn JH, Vizuete W, Heffron B, Lefer BL. Relationship between boundary layer heights and growth rates with ground-level ozone in Houston, Texas. *J Geophys Res Atmos* 2014;119. [2013]D020473.
- Hao JM, Wang LT, Li L, Hu JN, Yu XC. Air pollutants contribution and control strategies of energy-use related sources in Beijing. *Sci China Ser D* 2005;48:138–46.
- He HZ, Zhang FQ. Diurnal variations of warm-season precipitation over Northern China. *Mon Weather Rev* 2010;138:1017–25.
- He KB, Yang FM, Ma YL, Zhang Q, Yao XH, Chan CK, et al. The characteristics of PM_{2.5} in Beijing, China. *Atmos Environ* 2001;35:4959–70.
- Hong SY, Dudhia J, Chen SH. A revised approach to ice microphysical processes for the bulk parameterization of clouds and precipitation. *Mon Weather Rev* 2004;132:103–20.
- Hong SY, Noh Y, Dudhia J. A new vertical diffusion package with an explicit treatment of entrainment processes. *Mon Weather Rev* 2006;134:2318–41.
- Hu XM, Nielsen-Gammon JW, Zhang FQ. Evaluation of three planetary boundary layer schemes in the WRF model. *J Appl Meteorol Climatol* 2010a;49:1831–44.
- Hu XM, Sigler JM, Fuentes JD. Variability of ozone in the marine boundary layer of the equatorial Pacific Ocean. *J Atmos Chem* 2010b;66:117–36.
- Hu XM, Doughty DC, Sanchez KJ, Joseph E, Fuentes JD. Ozone variability in the atmospheric boundary layer in Maryland and its implications for vertical transport model. *Atmos Environ* 2012;46:354–64.
- Hu XM, Klein PM, Xue M, Zhang FQ, Doughty DC, Forkel R, et al. Impact of the vertical mixing induced by low-level jets on boundary layer ozone concentration. *Atmos Environ* 2013a;70:123–30.
- Hu XM, Klein PM, Xue M, Lundquist JK, Zhang FQ, Qi YC. Impact of low-level jets on the nocturnal urban heat island intensity in Oklahoma City. *J Appl Meteorol Climatol* 2013b;52:1779–802.
- Hu XM, Klein PM, Xue M. Evaluation of the updated YSU planetary boundary layer scheme within WRF for wind resource and air quality assessments. *J Geophys Res Atmos* 2013c;118:10490–505.
- Hu XM, Klein PM, Xue M, Shapiro A, Nallapareddy A. Enhanced vertical mixing associated with a nocturnal cold front passage and its impact on near-surface temperature and ozone concentration. *J Geophys Res Atmos* 2013d;118:2714–28.
- Hu J, Wang Y, Ying Q, Zhang H. Spatial and temporal variability of PM_{2.5} and PM₁₀ over the North China Plain and the Yangtze River Delta, China. *Atmos Environ* 2014;95:598–609.
- Huang JP, Zhou CH, Lee XH, Bao YX, Zhao XY, Fung J, et al. The effects of rapid urbanization on the levels in tropospheric nitrogen dioxide and ozone over East China. *Atmos Environ* 2013;77:558–67.
- Ji DS, Wang YS, Wang LL, Chen LF, Hu B, Tang GQ, et al. Analysis of heavy pollution episodes in selected cities of northern China. *Atmos Environ* 2012;50:338–48.
- Ji D, Li L, Wang Y, Zhang J, Cheng M, Sun Y, et al. The heaviest particulate air-pollution episodes occurred in northern China in January, 2013: insights gained from observation. *Atmos Environ* 2014;92:546–56.
- Koch SE, Zhang FQ, Kaplan ML, Lin YL, Weglarz R, Trexler CM. Numerical simulations of a gravity wave event over CCOPE. Part III: the role of a mountain-plains solenoid in the generation of the second wave episode. *Mon Weather Rev* 2001;129:909–33.
- Lang JL, Cheng SY, Li JB, Chen DS, Zhou Y, Wei X, et al. A monitoring and modeling study to investigate regional transport and characteristics of PM_{2.5} pollution. *Aerosol Air Qual Res* 2013;13:943–56.
- Lanicci JM, Warner TT. A synoptic climatology of the elevated mixed-layer inversion over the southern great-plains in spring. I. Structure, dynamics, and seasonal evolution. *Weather Forecast* 1991;6:181–97.
- Lanicci JM, Warner TT. A case study of lid evolution using analyses of observational data and a numerical model simulation. *Weather Forecast* 1997;12:228–52.
- Lin W, Xu X, Zhang X, Tang J. Contributions of pollutants from north china plain to surface ozone at the Shangdianzi GAW station. *Atmos Chem Phys* 2008;8:5889–98.
- Lin WL, Xu XB, Ge BZ, Zhang XC. Characteristics of gaseous pollutants at Gucheng, a rural site southwest of Beijing. *J Geophys Res Atmos* 2009;114:D00G1. <http://dx.doi.org/10.1029/2008JD010339>.
- Liu XD, Bai AJ, Liu CH. Diurnal variations of summertime precipitation over the Tibetan Plateau in relation to orographically-induced regional circulations. *Environ Res Lett* 2009;4:045203. <http://dx.doi.org/10.1088/1748-9326/4/4/045203>.
- Liu XG, Li J, Qu Y, Han T, Hou L, Gu J, et al. Formation and evolution mechanism of regional haze: a case study in the megacity Beijing, China. *Atmos Chem Phys* 2013;13:4501–14.
- Luke WT, Dickerson RR, Ryan WF, Pickering KE, Nunnermacker LJ. Tropospheric chemistry over the lower Great-Plains of the United-States. 2. Trace gas profiles and distributions. *J Geophys Res Atmos* 1992;97:20647–70.
- Ma MJ, Pu ZX, Wang SG, Zhang Q. Characteristics and numerical simulations of extremely large atmospheric boundary-layer heights over an arid region in North-west China. *Bound-Lay Meteorol* 2011a;140:163–76.
- Ma ZQ, Zhang XL, Xu J, Zhao XJ, Meng W. Characteristics of ozone vertical profile observed in the boundary layer around Beijing in autumn. *J Environ Sci (China)* 2011b;23:1316–24.
- Ma JZ, Wang W, Chen Y, Liu HJ, Yan P, Ding GA, et al. The IPAC-NC field campaign: a pollution and oxidation pool in the lower atmosphere over Huabei, China. *Atmos Chem Phys* 2012a;12:3883–908.
- Ma JZ, Xu XB, Zhao CS, Yan P. A review of atmospheric chemistry research in China: photochemical smog, haze pollution, and gas-aerosol interactions. *Adv Atmos Sci* 2012b;29:1006–26.
- Ma ZQ, Xu HH, Meng W, Zhang XL, Xu J, Liu Q, et al. Vertical ozone characteristics in urban boundary layer in Beijing. *Environ Monit Assess* 2013;185:5449–60.
- May PT, Wilczak JM. Diurnal and Seasonal-variations of boundary-layer structure observed with a radar wind profiler and RASS. *Mon Weather Rev* 1993;121:673–82.
- Meng ZY, Xu XB, Yan P, Ding GA, Tang J, Lin WL, et al. Characteristics of trace gaseous pollutants at a regional background station in Northern China. *Atmos Chem Phys* 2009;9:927–36.
- Mlawer EJ, Taubman SJ, Brown PD, Iacono MJ, Clough SA. Radiative transfer for inhomogeneous atmospheres: RRTM, a validated correlated-k model for the longwave. *J Geophys Res Atmos* 1997;102:16663–82.
- Nielsen-Gammon JW, Powell CL, Mahoney MJ, Angevine WM, Senff C, White A, et al. Multisensor estimation of mixing heights over a coastal city. *J Appl Meteorol Climatol* 2008;47:27–43.
- Pagnotti V. A meso-meteorological feature associated with high ozone concentrations in the Northeastern United States. *JAPCA* 1987;37:720–2.
- Quan JN, Gao Y, Zhang Q, Tie XX, Cao JJ, Han SQ, et al. Evolution of planetary boundary layer under different weather conditions, and its impact on aerosol concentrations. *Particology* 2013;11:34–40.
- Quan J, Tie X, Zhang Q, Liu Q, Li X, Gao Y, et al. Characteristics of heavy aerosol pollution during the 2012–2013 winter in Beijing, China. *Atmos Environ* 2014;88:83–9.
- Ryan WF, Dickerson RR, Huffman GJ, Luke WT. Tropospheric chemistry over the lower Great-Plains of the United-States. 1. Meteorology. *J Geophys Res Atmos* 1992;97:17963–84.
- Sandeep A, Rao TN, Ramkiran CN, Rao SVB. Differences in atmospheric boundary-layer characteristics between wet and dry episodes of the Indian summer monsoon. *Bound-Lay Meteorol* 2014;1–20. <http://dx.doi.org/10.1007/s10546-014-9945-z>.
- Seaman NL, Michelson SA. Mesoscale meteorological structure of a high-ozone episode during the 1995 NARSTO-Northeast study. *J Appl Meteorol* 2000;39:384–98.

- Stubi R, Levrat G, Hoegger B, Viatte P, Staehelin J, Schmidlin FJ. In-flight comparison of Brewer–Mast and electrochemical concentration cell ozonesondes. *J Geophys Res Atmos* 2008;113. <http://dx.doi.org/10.1029/2007JD009091>. [D13302].
- Su FQ, Yang MZ, Zhong JH, Zhang ZG. The effects of synoptic type on regional atmospheric contamination in north China. *Res Environ Sci* 2004;17:16–20. (in Chinese).
- Sun JH, Zhang FQ. Impacts of mountain–plains solenoid on diurnal variations of rainfalls along the Mei–Yu front over the East China Plains. *Mon Weather Rev* 2012;140:379–97.
- Sun YL, Zhuang GS, Tang AH, Wang Y, An ZS. Chemical characteristics of PM_{2.5} and PM₁₀ in haze–fog episodes in Beijing. *Environ Sci Technol* 2006;40:3148–55.
- Tripoli GJ, Cotton WR. Numerical study of an observed orogenic mesoscale convective system.2. Analysis of governing dynamics. *Mon Weather Rev* 1989;117:305–28.
- Wang Y, Hao J, McElroy MB, Munger JW, Ma H, Chen D, et al. Ozone air quality during the 2008 Beijing Olympics: effectiveness of emission restrictions. *Atmos Chem Phys* 2009;9:5237–51.
- Wang F, Chen DS, Cheng SY, Li JB, Li MJ, Ren ZH. Identification of regional atmospheric PM₁₀ transport pathways using HYSPLIT, MM5-CMAQ and synoptic pressure pattern analysis. *Environ Model Softw* 2010a;25:927–34.
- Wang T, Nie W, Gao J, Xue LK, Gao XM, Wang XF, et al. Air quality during the 2008 Beijing Olympics: secondary pollutants and regional impact. *Atmos Chem Phys* 2010b;10:7603–15.
- Wang YH, Hu B, Tang GQ, Ji DS, Zhang HX, Bai JH, et al. Characteristics of ozone and its precursors in Northern China: a comparative study of three sites. *Atmos Res* 2013a;132:450–9.
- Wang ZB, Hu M, Wu ZJ, Yue DL, He LY, Huang XF, et al. Long-term measurements of particle number size distributions and the relationships with air mass history and source apportionment in the summer of Beijing. *Atmos Chem Phys* 2013b;13:10159–70.
- Wang D, Hu J, Xu Y, Lv D, Xie X, Kleeman M, et al. Source contributions to primary and secondary inorganic particulate matter during a severe wintertime PM_{2.5} pollution episode in Xi'an, China. *Atmos Environ* 2014;97(0):182–94. <http://dx.doi.org/10.1016/j.atmosenv.2014.08.020>.
- Warner TT, Sheu RS. Multiscale local forcing of the Arabian Desert daytime boundary layer, and implications for the dispersion of surface-released contaminants. *J Appl Meteorol* 2000;39:686–707.
- Wei P, Cheng SY, Li JB, Su FQ. Impact of boundary-layer anticyclonic weather system on regional air quality. *Atmos Environ* 2011;45:2453–63.
- Westra D, Steeneveld GJ, Holtslag AAM. Some observational evidence for dry soils supporting enhanced relative humidity at the convective boundary layer top. *J Hydrometeorol* 2012;13:1347–58.
- Wolyn PG, Mckee TB. The mountain plains circulation east of a 2-km-high north south barrier. *Mon Weather Rev* 1994;122:1490–508.
- Xu J, Ma JZ, Zhang XL, Xu XB, Xu XF, Lin WL, et al. Measurements of ozone and its precursors in Beijing during summertime: impact of urban plumes on ozone pollution in downwind rural areas. *Atmos Chem Phys* 2011a;11(23):12241–52. <http://dx.doi.org/10.5194/acp-11-12241-2011>.
- Xu WY, Zhao CS, Ran L, Deng ZZ, Liu PF, Ma N, et al. Characteristics of pollutants and their correlation to meteorological conditions at a suburban site in the North China Plain. *Atmos Chem Phys* 2011b;11:4353–69.
- Yang L, Wu Y, Davis JM, Hao JM. Estimating the effects of meteorology on PM_{2.5} reduction during the 2008 Summer Olympic Games in Beijing, China. *Front Environ Sci Eng* 2011;5:331–41.
- Ye DZ. Some characteristics of the summer circulation over the Qinghai–Xizang (Tibet) plateau and its neighborhood. *Bull Am Meteorol Soc* 1981;62:14–9.
- Zaitchik BF, Evans JP, Smith RB. Regional impact of an elevated heat source: the Zagros Plateau of Iran. *J Clim* 2007;20:4133–46.
- Zhang FQ, Koch SE. Numerical simulations of a gravity wave event over CCOPE. Part II: waves generated by an orographic density current. *Mon Weather Rev* 2000;128:2777–96.
- Zhang FQ, Bei NF, Nielsen-Gammon JW, Li GH, Zhang RY, Stuart A, et al. Impacts of meteorological uncertainties on ozone pollution predictability estimated through meteorological and photochemical ensemble forecasts. *J Geophys Res Atmos* 2007;112(D4). <http://dx.doi.org/10.1029/2006jd007429>. [D04304].
- Zhang XY, Wang YQ, Lin WL, Zhang YM, Zhang XC, Gong S, et al. Changes of atmospheric composition and optical properties over Beijing 2008 Olympic monitoring campaign. *Bull Am Meteorol Soc* 2009a;90:1633–51.
- Zhang Q, Ma XC, Tie XX, Huang MY, Zhao CS. Vertical distributions of aerosols under different weather conditions: analysis of in-situ aircraft measurements in Beijing, China. *Atmos Environ* 2009b;43:5526–35.
- Zhang JP, Zhu T, Zhang QH, Li CC, Shu HL, Ying Y, et al. The impact of circulation patterns on regional transport pathways and air quality over Beijing and its surroundings. *Atmos Chem Phys* 2012a;12:5031–53.
- Zhang H, Li JY, Ying Q, Yu JZ, Wu D, Cheng Y, et al. Source apportionment of PM_{2.5} nitrate and sulfate in China using a source-oriented chemical transport model. *Atmos Environ* 2012b;62:228–42.
- Zhang YC, Sun JH, Fu SM. Impacts of diurnal variation of mountain–plain solenoid circulations on precipitation and vortices east of the Tibetan Plateau during the Mei–Yu season. *Adv Atmos Sci* 2014;31:139–53.
- Zhao PS, Zhang XL, Xu XF, Zhao XJ. Long-term visibility trends and characteristics in the region of Beijing, Tianjin, and Hebei, China. *Atmos Res* 2011;101:711–8.
- Zhao XJ, Zhao PS, Xu J, Meng W, Pu WW, Dong F, et al. Analysis of a winter regional haze event and its formation mechanism in the North China Plain. *Atmos Chem Phys* 2013;13:5685–96.